



First Experimental Demonstration of Machine Learning-Based Tuning on the PSI Injector 2 Cyclotron

M. Haj Tahar ^{*}, W. Joho, E. Solodko, M. Bocchio, S. Marquie, and M. Busch
Transmutex SA, Vernier, Switzerland

A. Barchetti, J. Grillenberger, J. Snuerink , and M. Schneider
Paul Scherrer Institut, Villigen, Switzerland

Reliable operation of high-power proton cyclotrons is a critical requirement for Accelerator Driven Systems (ADS) and other large-scale applications. Beam tuning in such machines is traditionally performed manually, a process that can be slow, non-optimal, and difficult to execute in the presence of faults or changing conditions. To address this, we developed and deployed a machine learning (ML) based tuning framework on the Injector 2 cyclotron at PSI, chosen as an ideal testbed for high-power operation. The system combined a tailored reinforcement learning algorithm with real-time diagnostics and control, and incorporated accelerator-physics inspired adaptations such as an overshoot strategy that reduced magnetic field settling times by nearly a factor of six. Over an extensive 12-day operational test campaign, relatively long in the context of real-time ML experiments, the ML agent successfully tuned the machine across multiple operating points, achieving convergence within hours and maintaining stable beam extraction with reduced losses. Beyond initial tuning, the system was also operated in evaluation mode overnight, where it autonomously monitored and corrected the machine to compensate for drifts, demonstrating robustness and long-term stability. Crucially, the learned policy generalized reliably from low-current training to higher-current operation, underscoring its scalability. These results constitute the first demonstration of ML-assisted tuning on a high-power cyclotron, with direct relevance to ADS-class drivers.

I. INTRODUCTION

The High Intensity Proton Accelerator (HIPA) complex at the Paul Scherrer Institut (PSI) has been in operation since 1974, and today delivers the most intense continuous-wave proton beam worldwide, with an average power of 1.42 MW produced by a two-stage cyclotron system [1]. In the first stage, Injector 2 accelerates protons from 0.87 MeV, provided by a Cockcroft–Walton DC linear accelerator, up to 72 MeV. The second stage, the 590 MeV ring cyclotron, then boosts the beam to its final energy, with a maximum average current of 2.4 mA. After extraction, which is achieved with efficiencies exceeding 99.98%, the beam is transported to multiple target stations for meson and neutron production [2], enabling world-class programs in particle, nuclear, and materials science. Cyclotron-based proton drivers, as demonstrated at PSI, are a well-proven technology, combining compactness with high energy efficiency. These qualities make them particularly attractive for future large-scale applications such as Accelerator Driven Systems (ADS) [3, 4].

Within this context, Transmutex SA is developing an ADS concept aimed at generating clean energy while simultaneously reducing the long-term radiotoxicity of nuclear waste. The architectural similarities between the HIPA cyclotrons and the envisioned ADS driver make PSI’s Injector 2 an ideal testbed to investigate the control strategies and automation capabilities required for such systems.

Looking beyond current applications, ADS place uniquely stringent requirements on the reliability of high-power proton drivers. Target applications in nuclear waste transmutation or energy generation demand continuous operation with failure rates two orders of magnitude lower than those achieved today. To reach such performance, not only must the hardware of cyclotrons be robust, but new operational strategies must be developed to rapidly compensate for inevitable component failures. At PSI, proof-of-principle experiments have already demonstrated that, in the event of a cavity failure in the 590 MeV ring cyclotron, beam delivery can be recovered within minutes by retuning the remaining cavities [5]. While this demonstrates feasibility, a recovery on the order of minutes falls short of the requirement for ADS-class facilities, where fault compensation must occur within only a few seconds. These results highlight the feasibility of fault compensation but also reveal a critical bottleneck: the lack of reliable, automated tuning tools capable of acting on the time scales demanded by ADS-class facilities.

^{*}Electronic address: malek@transmutex.com

Machine Learning (ML) has emerged as a promising candidate to address this challenge [6]. By leveraging data-driven models and adaptive optimization, ML offers the potential to automate cyclotron tuning, compensate for drifts, and adapt to changing operational conditions in real time. While ML approaches have been explored in linear accelerators and light sources, their application to high-power cyclotrons remains largely unexplored [7–10]. To fill this gap, PSI Injector 2 was chosen as an experimental testbed, combining the complexity of a high-power machine with the flexibility needed for R&D.

The present work reports on the first experimental demonstration of ML-assisted tuning on Injector 2. A tailored Reinforcement Learning (RL) framework was integrated with real-time diagnostics and control of the machine, enabling the agent not only to converge on optimal settings within hours but also to maintain stable operation during overnight evaluation runs by autonomously compensating drifts. This effort was carried out over an extensive 12-day experimental campaign, which is remarkably long in the context of real-time ML control studies. The results of this campaign provide an essential step towards establishing ML-based control as a reliable tool for fault compensation and robust operation in ADS-class drivers.

To move beyond proof-of-concept and towards reliable deployment, the Injector 2 campaign was carefully crafted to address a set of fundamental questions. At the technical level, these include identifying which actuators and diagnostics provide the greatest leverage for beam stabilization, how the machine should be initialized before handing control to an ML agent, and what forms of surrogate modeling or pretraining are most effective in accelerating convergence. At the methodological level, the campaign explored how quickly an RL policy can converge in a real cyclotron, whether a model trained at low current generalizes to higher-intensity operation, how frequently retraining is required to counteract drifts, and to what extent transfer learning across turn numbers can reduce setup time. At the heart of this effort lies the central question: can a cyclotron be operated reliably with limited human intervention, using ML-based control strategies that meet the stringent demands of ADS-class drivers?

The remainder of this paper is organized as follows. Section II describes the Injector 2 cyclotron and its diagnostics, together with the control framework used for the experiments. Section III presents an analysis of historical data and feature engineering choices that informed the ML environment design. Section IV outlines the overall tuning strategy and campaign design. In Section V, the turn- and current-dependent beam dynamics are characterized using radial probe and Jacobian measurements, providing the physics context for the tuning challenge. Section VI discusses the adaptations required to integrate accelerator physics constraints into the ML framework, including the overshoot strategy and reward shaping; in particular, the overshoot strategy was found to accelerate the tuning process by nearly a factor of six. Section VII details the RL methodology employed, while Section VIII reports the experimental results, covering low-current training, overnight evaluation, and generalization to higher beam currents. Section IX presents the conclusions and outlines the roadmap toward scaling the demonstrated methodology to the HIPA complex and future ADS-class accelerator drivers.

II. EXPERIMENTAL SETUP

Injector 2 is a four-sector separated-sector cyclotron designed to accelerate protons from an injection energy of 870 keV to a final energy of 72 MeV [11, 12]. Its principal components include four large sector magnets (SM1–SM4), two double-gap RF resonators (CI1 and CI3), and two single-gap resonators (CI2 and CI4). A schematic layout of the machine with the main diagnostics is shown in Fig. 1.

The proton beam enters Injector 2 from the vertical pre-injection line and is bent into the median plane by the AWD dipole magnet. It then passes through a conical injection channel in the first sector magnet (SM1), which is equipped with a dedicated trim coil to guide the first turn. During the first six turns, a system of collimators minimizes beam halo and ensures a well-centered trajectory. Additional fine control at this stage is provided by trim coils TI1A/B and TI2 located in SM1 and SM3.

A. Sector Magnets, Trim Coils, and Resonators

Each sector magnet is powered by a pair of main coils (AIHS) connected in series. These coils generate the primary magnetic field and play a central role in shaping the beam trajectory, thereby defining the overall particle orbit. Nine pairs of trim coils (TI3–TI11), mounted above and below the median plane on one side of the pole, provide localized magnetic field corrections that are indispensable for precise orbit control and efficient extraction.

Beam acceleration is achieved by four RF resonators: two double-gap (CI1 and CI3) and two single-gap (CI2 and CI4). CI1 is critical for defining the first-turn trajectory and is therefore kept fixed during tuning. In combination, the resonators determine the per-turn energy gain and the radial position of successive turns. The AIHS main coils, trim coils, and resonator voltages were all made available as controllable channels for the ML agent.

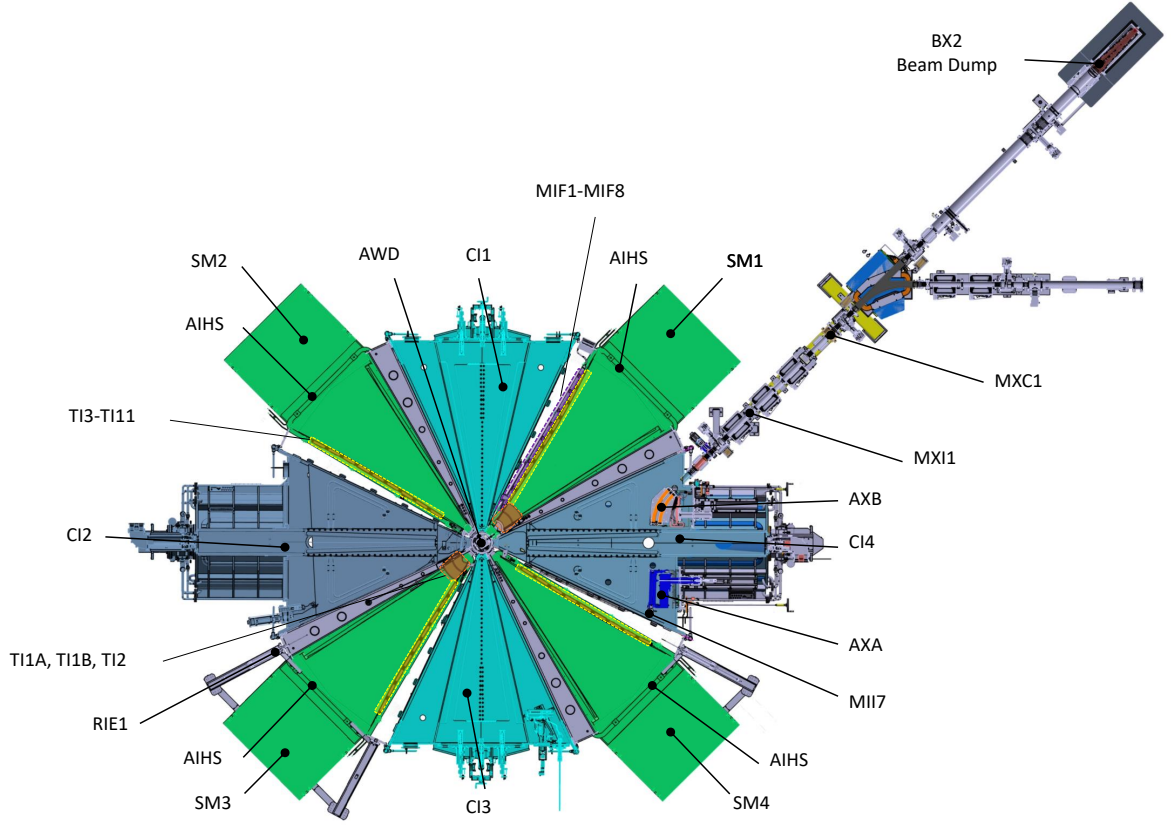


FIG. 1: Injector 2 Cyclotron experiment setup with key diagnostics.

B. Beam Diagnostics

The following diagnostics were employed during the ML campaign:

- MIF probes (MIF1–MIF8): Eight phase probes in the first sector, providing phase information at different beam energies from injection to extraction. These were the primary reward signals.
- Loss monitors: Ionization chambers MII7 (before the extraction septum) and MXI1 (downstream), plus the KXAI collimators at the septum entrance.
- MXC1: high-resolution current transformer downstream of the septum, monitoring extracted beam intensity.
- Radial probe (RIE1): movable probe system used to obtain radial beam profiles in the extraction region (last 7 turns). This is a slow measurement applied for beam characterization rather than in the experimental ML feedback loop.

III. HISTORICAL DATA ANALYSIS AND FEATURE ENGINEERING

A. Review of archived operational data

The project relied on historical sensor data recorded by PSI’s archival systems. These archives log measurements from a wide range of sensors integrated into HIPA subsystems, providing long-term records of operational conditions and system stability. Data extraction was performed with a dedicated Python library developed at PSI to interface with the archival infrastructure.

A characteristic feature of the archival data is the irregularity of time steps, due to differing update rates across channels. While some parameters are logged at fixed intervals, others are updated only when changes occur. To standardize the dataset, all channels were resampled to a fixed 200 ms interval, using the most recent value available at each time step. This procedure yields a consistent dataset that reflects the operational state of the accelerator at uniform temporal resolution.

The extracted dataset covers a broad range of parameters, nearly all originating from Injector 2, with the exception of the downstream losses and beam current measurements.

The choice of historical intervals for data extraction was guided by the need to match the expected machine configuration during experimental deployment. Since resonator setups strongly affect beam dynamics, only periods corresponding to similar configurations were considered. Three representative periods were identified:

- May 2023 - December 2023: operation with two double-gap resonators and one flattop cavity (low voltage, treated as equivalent to two double-gap configuration).
- May 2024 - July 2024: operation with two double-gap resonators.
- August 2024 - December 2024: operation with two double-gap resonators and one single-gap resonator.

These intervals ensured that the training dataset reflected machine states consistent with those expected during ML validation.

B. Features selection and augmentation

From the full channel set, a refined subset was selected based on data quality, physical relevance, and model performance in preliminary studies. The final input space included: TIs (trim coil currents), CIVs (resonator voltages), AIHS (main coil current), aggregated magnet and air temperatures, MIFs (beam phases), MII7 and MXI1 ionization chambers, and MXC1 beam current. These were complemented with engineered features such as estimates of the turn number and a set of stability indicators, the latter mostly defined by MXC1 ripple. This combination preserved physical interpretability while enhancing model performance.

A comprehensive sequence of preprocessing steps was applied to produce a clean and representative dataset for training the surrogate model. After these procedures, the resulting dataset comprised 27.3 million datapoints, corresponding to 63.2 days of Injector 2 operation.

C. Correlation analysis

Correlation matrices were computed across the selected dataset to validate physical consistency and identify dominant dependencies. The analysis revealed:

- Strong correlations among magnet temperature sensors and among air temperature sensors, justifying their aggregation into mean values.
- Clear correlations between resonator voltages and MIF signals, reflecting the dependence of beam phase on energy gain per turn.
- Secondary correlations between trim coil currents and MIFs, consistent with their influence on radial orbit control.

These results confirm that the surrogate modeling task is dominated by deterministic physical relations, while also supporting feature reduction without loss of essential information. A representative correlation heatmap is provided in Appendix A (Fig. 16).

IV. TUNING STRATEGY AND CAMPAIGN OVERVIEW

The deployment of ML control in Injector 2 was carefully planned to balance safety, diagnostic coverage, and systematic exploration of machine behavior. A beam current of 20 μA was selected as the reference for training, providing reliable phase measurements at sufficiently low beam power to minimize activation risks in case of instability.

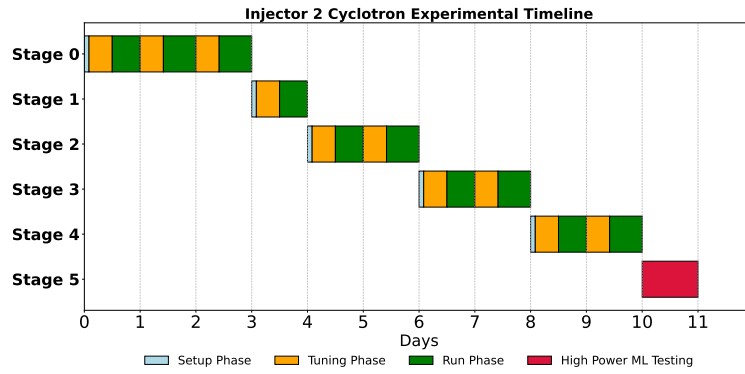


FIG. 2: Phase Breakdown of Inj 2 Cyclotron Experiment; the experiment took place from Apr 28, 2025 until May 8th, 2025 i.e., for a total of 11 days.

At this current, the beam size remained small enough to allow wide action exploration, yet the signal quality was adequate to meaningfully characterize losses and phase shifts.

The tuning strategy was organized around two classes of actuators. The main coil power supply current for the magnetic field (AIHS) and the voltage of resonator 3 (CI3V) were identified as the dominant parameters controlling global beam conditions, specifically the radial trajectory and the extraction energy. Both were included in the RL action space, but their operational boundaries were carefully determined in advance by manual scans to ensure sufficient headroom before interlocks. All twelve remaining trim coils were also available to the RL agent, primarily to compensate for local phase deviations. Reward shaping was employed to discourage excessive trim coil usage, ensuring that corrections reflected genuine improvements in global conditions rather than overcompensation.

The campaign itself targeted five distinct machine configurations, each corresponding to a specific turn number, adjusted by varying the peak voltages of resonators 2 and 4. The corresponding resonator settings are summarized in Table I. These configurations were deliberately selected to span the three operational scenarios of Injector 2: nominal operation with four resonators, reduced operation with three resonators, and a degraded mode with only two resonators. This allowed us to systematically investigate how the ML agent adapts its tuning strategy under both nominal and failure-like conditions.

TABLE I: Resonator configuration per experimental stage. Listed are the peak voltages of the four resonators (in kVp) for each turn number.

Stage	Turn number	Resonator setup (kVp)			
		Res 1	Res 2	Res 3	Res 4
0	72	430	429	451	0
1	73	430	401	449	0
2	74	430	371	448	0
3	89	430	0	449	0
4	60	430	428	448	428

Each stage of the campaign followed a structured daily cycle. During the morning setup phase, operators configured the machine to the target turn number, optimized the beam at nominal current (2 mA), and probe measurements were performed at various currents. Low-current ML training runs were then performed during the daytime, typically lasting several hours. Following training, the ML agent was left in autonomous control during evening and overnight periods, providing a stringent test of stability, drift compensation, and interlock recovery over many hours of operation (12 hours). A final high-current validation stage 5 extended ML control into the milliampere regime to evaluate scalability of the learned policies. The overall timeline of the campaign is illustrated in Fig. 2, which shows the sequential execution of setup, training, and long-term evaluation phases across the 11-day experimental run. An additional one day, prior to experiment, was dedicated for setup tests. This phased execution strategy ensured that each configuration was benchmarked against operator-validated references, that ML training was conducted in safe regimes, and that robustness was tested under realistic conditions, including day-to-night transitions. In total, the campaign covered five turn numbers across multiple resonator configurations, produced hundreds of hours of machine learning operation, and generated a comprehensive dataset for offline analysis.

V. TURN AND CURRENT-DEPENDENT BEAM DYNAMICS: RADIAL PROFILES AND JACOBIAN EVOLUTION

Cyclotron beam dynamics exhibit strong dependence on both the number of turns and the operating beam current. This section summarizes the empirical observations obtained during the Injector 2 campaign, combining radial probe measurements with sensitivity (Jacobian) analyses to quantify how the response of the machine evolves under different conditions.

A. Beam setup and turn-dependent operation

For each selected turn number configuration, the reference operating point was established at a beam current of 2 mA, which represents the maximum achievable current even in reduced-resonator modes. Daily operations began with low-current operator-led adjustments of resonator voltages and coil settings to configure the desired turn number, followed by optimization at 2 mA to ensure stable transmission and extraction efficiency. In certain cases, additional interventions such as collimator repositioning (KIP4, KIR1L) or adjustment of the extraction septum (AXA) were required to restore beam quality.

The complexity of tuning was found to increase with the number of turns, particularly when fewer resonators were active. Configurations with only two active resonators (e.g. 89 turns) exhibited the highest sensitivity, where small deviations in magnetic field or RF voltage led to rapid beam change and frequent interlocks. A summary of the tuning requirements across turn numbers is given in Table II, highlighting the longer setup times required in these challenging configurations. Such operator-dependent procedures are not sustainable for ADS-class drivers, thereby motivating the development of ML-based automated tuning methods.

TABLE II: Summary of operator-led fine-tuning procedures across turn configurations.

Turn change	Interlocks activated	Tuning time
72 → 73	3	10 min
73 → 74	3	9 min
74 → 89	7	47 min
89 → 60	0	10 min

B. Radial probe measurements

To quantify the radial size of the extracted beam, Gaussian fits were applied to the RIE1 probe profiles across beam currents from 20 μ A to 2 mA and for multiple turn numbers. The analysis reveals a clear current-dependent broadening of the radial beam size, consistent with earlier observations at injector II [13, 14], and with systematic differences between turns. To obtain a more representative measure of the extraction region, the radial width was averaged over the last three turns, which smooths fluctuations due to coherent betatron oscillations while preserving the physical envelope. The results, shown in Fig. 3a, demonstrate consistent beam growth with current and turn dependence.

Comparison with BMAD self-consistent space-charge tracking simulations confirms the observed slope change around 1 mA, pointing to the onset of collective effects [15]. The close agreement between experiment and simulation (Fig. 3b) provides confidence in the physical interpretation and establishes a solid basis for benchmarking ML-guided tuning strategies under varying current and turn conditions.

C. Jacobian analysis and sensitivity evolution

To quantify how control actuators affect the phase probes, turn-dependent Jacobian matrices were measured using finite-difference perturbations [16]. Each control parameter (AIHS, CI3V, and the twelve trim coils) was perturbed individually, with stabilization periods inserted between perturbations to ensure reproducible phase readings. The resulting Jacobians capture the partial derivatives of the measured phases (MIF1–MIF8) with respect to each actuator.

The measured Jacobians exhibited strong dependence on the turn number. In particular, the sensitivity of the outer probes (MIF4–MIF8) to changes in AIHS increased markedly at higher turn numbers. This behavior reflects the underlying beam dynamics: reducing the voltage of resonators 2 and 4 forces the beam to take additional turns at

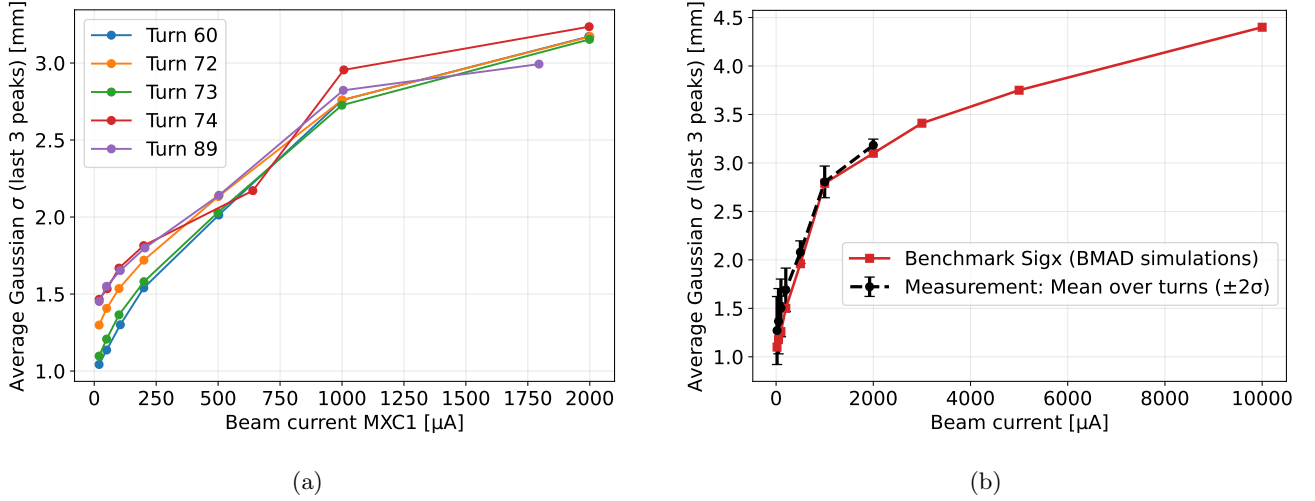


FIG. 3: (a) Average radial beam size at extraction versus current, for various turn numbers (averaged over the last three turns). (b) Comparison of the measured average σ , obtained by averaging over all turn numbers shown in (a) (mean $\pm 2\sigma$), with space-charge tracking simulations.

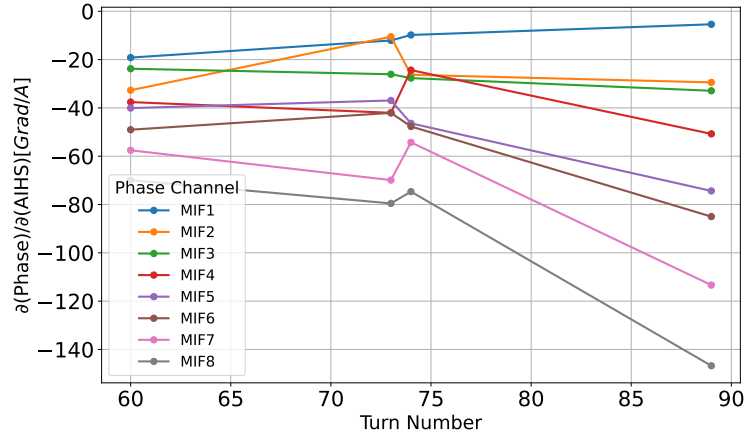


FIG. 4: Sensitivity of phases to AIHS change with respect to the turn number, for a perturbation amplitude of 0.02 Amp.

large radii, where changes in the main magnetic field have a magnified effect. Conversely, early probes (MIF1–MIF3) showed only weak dependence, consistent with their location near injection. Similar trends were observed for specific trim coils, such as TI11 and TI10, whose influence on the phase distribution varied significantly with turn number. Representative sensitivities are shown in Fig. 4.

Beyond turn dependence, the Jacobians also displayed strong sensitivity to the working point. Even for fixed perturbation amplitudes, the measured responses varied significantly depending on the resonator and coil settings chosen to achieve a given turn number. This working-point dependence reflects the nonlinear character of the machine and emphasizes the need for adaptive, data-driven control strategies.

D. Implications for ML-based tuning

Together, the radial probe and Jacobian measurements demonstrate that the difficulty of cyclotron tuning increases systematically with both beam current and turn number. The system becomes more sensitive to small perturbations at outer radii, while space-charge effects contribute to beam broadening at higher currents. These findings motivate the staged design of the Injector 2 campaign: starting from low-current training runs, progressing turn by turn,

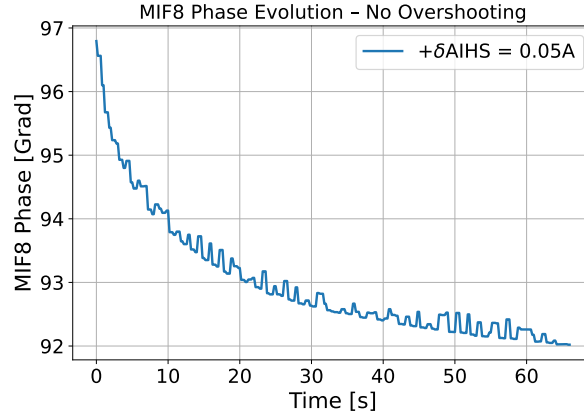


FIG. 5: MIF8 phase response following a $+0.05$ A step increase in AIHS current without overshooting. The system exhibits a slow exponential settling, requiring nearly 60 seconds to stabilize (turn 72).

and culminating in generalization tests at higher currents. They also provide critical guidance for ML integration, highlighting the need for agents capable of adapting to turn- and current-dependent response functions rather than assuming static machine behavior. Moreover, the response of the system is influenced by external factors such as the temperature of the magnets, underlining the importance of developing control policies that remain robust against slow drifts and environmental variations.

VI. ADAPTING ACCELERATOR PHYSICS FOR ML INTEGRATION

The successful deployment of machine learning in accelerator control requires more than sophisticated algorithms; it depends critically on adapting the underlying physics to become accessible, safe, and efficient for data-driven optimization. In Injector 2, a set of targeted modifications were introduced that made the machine's physical response compatible with RL, effectively bridging the gap between abstract policy learning and practical beam tuning. Two innovations were particularly decisive: an overshooting strategy that accelerated magnet settling times by nearly a factor of six, and a physics-informed reward design that aligned the agent's objectives with those of experienced operators.

A. Overshooting Strategy

One of the primary limitations for online control was the slow settling of the magnetic field following adjustments to the main magnet coil (AIHS). After a small current step, the associated MIF8 phase signal typically required close to 60 s to reach a steady state, as is shown in Fig. 5 severely limiting the number of agent-environment interactions achievable during training.

To accelerate this response, an overshooting scheme was implemented: each commanded current change was initially exceeded by 100% of the target perturbation and then reverted to the nominal value after a fixed interval of 7 s. As shown in Fig. 6, this approach reduced the effective settling time to approximately 10 s, representing nearly a sixfold improvement compared to the baseline response. The method was verified across a range of perturbation amplitudes and constrained to remain within interlock limits, ensuring safe operation while significantly increasing training throughput. A patent application has been submitted covering this overshooting strategy as applied to cyclotron magnetic field control.

B. Reward Shaping

To align the learning objective with accelerator performance and protection, a physics-informed reward function was designed. The total reward was expressed as:

$$R = R_{beam} + P_{trim} + P_{interlock} \quad (1)$$

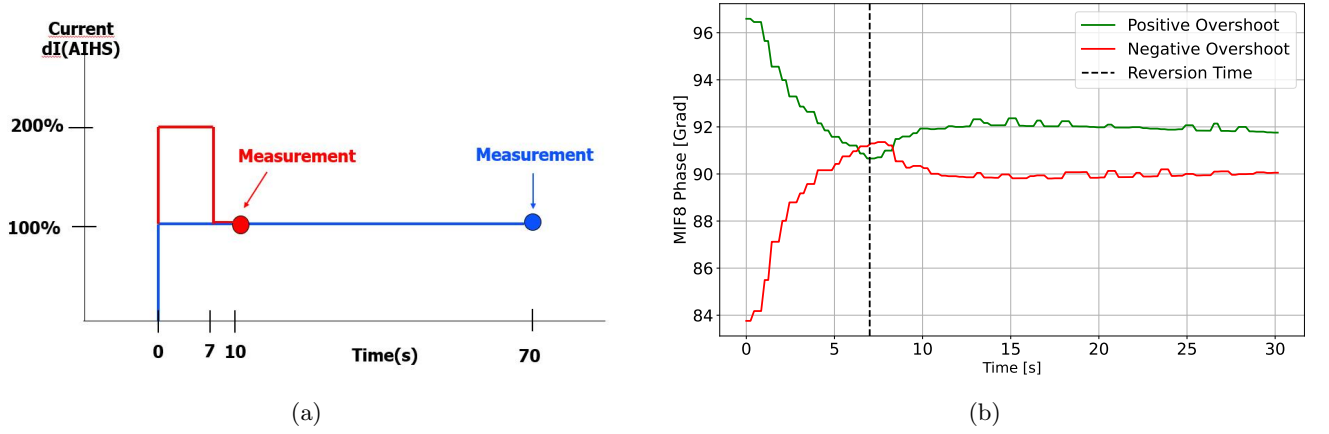


FIG. 6: (a) Main coil current change with (red) or without overshooting (blue). (b) MIF8 phase response to positive and negative overshooting with an AIHS final step of ± 0.05 A, using 100% overshoot and a 7-second reversion time (Turn 72).

where R_{beam} encodes beam quality, P_{trim} penalizes excessive use of trim coils, and $P_{interlock}$ enforces safety by strongly penalizing beam loss events. The central term is the weighted error between measured and reference beam phases at the eight MIF probes:

$$R_{phase} = \left(\sum_{i=1}^8 w_i (\phi_i - \phi_i^{ref})^2 \right)^{1/2}, \quad (2)$$

where ϕ_i is the measured phase at probe i , ϕ_i^{ref} is the corresponding reference, and w_i are weighting factors, with higher weights assigned to the outer probes (MIF6–MIF8) to reflect the importance of phase alignment near extraction, where the seen cavity voltage is nearly at its peak. Beam losses were incorporated through the deviation of the measured current loss signal ΔI_{loss} from its minimal reference value. The combined beam-related reward was then:

$$R_{beam} = -\frac{1}{2} \left[\tanh\left(\frac{R_{phase}}{10}\right) + \tanh\left(\frac{\Delta I_{loss}}{30}\right) \right]. \quad (3)$$

In addition trim-coil usage was penalised to discourage excessive local corrections:

$$P_{trim} = -\lambda \frac{1}{N} \sum_{j=1}^N |I_j|, \quad (4)$$

where I_j is the unnormalised current applied to trim coil j , $N = 12$ is the number of coils, and λ a scaling factor. This formulation ensures bounded contributions and avoids divergence during training.

The reward function was first implemented in a BMAD-based tracking environment, which provided a safe platform for systematic testing. These simulations confirmed that the chosen formulation was sensitive to physically meaningful deviations and yielded stable agent behavior. In particular, they allowed inspection of the RL agent's convergence time under different reward designs. Good convergence was defined as achieving successful tuning within fewer than 1000 timesteps, typically corresponding to the agent bringing the machine to the desired state in one or two corrective actions. The final reward formulation consistently met this criterion, ensuring both fast convergence and physically interpretable actions. This validation step was essential prior to deployment on the real machine.

The reward threshold of -0.08 was selected as a compromise between the intrinsic noise level of the phase diagnostics and the physics-informed definition of successful beam tuning. This value was fine-tuned using simulation studies to ensure consistent convergence behavior. In practice, the corresponding performance, phase errors of approximately $\pm 1^\circ$ and average trim-coil usage below 20% of their range, represents a physically meaningful criterion for optimal tuning equivalent to $R > -0.08$.

C. Interlock Handling

A layered interlock strategy was implemented in addition to the standard HIPA protection systems. The interlocks monitored three classes of signals: (i) the validity of the MIF phase measurements, (ii) the level of beam losses detected by KXAI, MII7, and MXI1, and (iii) the stability of the extracted current measured by MXC1. An interlock was issued whenever the MIF signals became invalid or out of range, whenever losses exceeded the predefined thresholds or returned undefined values, or whenever the MXC1 current deviated by more than 20% from its nominal value.

The interlock response followed a two-stage logic. In the first stage, the ML agent rolled back to the last known valid action with a small perturbation added to avoid repeated oscillation around the same point. If recovery was not achieved within the allowed window, a second interlock was raised. In this case, ML control was halted and the system transitioned into a safe mode, in which it remained until the MXC1 signal demonstrated stable behavior within 20% for at least 40 s.

All interlock events were automatically logged together with their timestamps, type (single or double), and root cause, which allowed a detailed analysis of agent behavior under fault conditions.

VII. REINFORCEMENT LEARNING METHODOLOGY

The reinforcement learning framework was implemented using the Twin Delayed Deep Deterministic Policy Gradient (TD3) algorithm, which is well suited for continuous action spaces and has been shown to provide stable convergence in noisy environments [17, 18]. A custom OpenAI Gym-compatible environment was developed to interface the agent with Injector 2, ensuring modularity and reproducibility of the experimental framework.

Injector 2 is operated with the Experimental Physics and Industrial Control System (EPICS). A dedicated Linux server running PyEPICS provided real-time access to process variables (PVs), enabling safe, low-latency communication between the ML agent and the accelerator subsystems.

The action space consisted of 14 normalized variables: the 12 trim coils, the main correction coil (AIHS), and the CI3V resonator voltage. The observation space included MIF1-MIF8 phase probes, beam loss monitors (MII7 and MXI1), turn number, beam current (MXC1), and environmental metrics such as magnet temperatures (MIT, MIT_M). All variables were normalized to the range $[-1, 1]$ to ensure balanced scaling and efficient training.

The agent's objective was to minimize the weighted deviation between the measured phase profile and a predefined reference, while simultaneously penalizing beam losses and excessive trim coil usage (see Sec. VIB). Interlock conditions defined by abrupt beam current drops, anomalous losses, or invalid phase signals, resulted in large negative rewards, enforcing safe exploration during training.

The slow response of the main coil (AIHS) was addressed through a dedicated overshooting strategy (Sec. VIA), which reduced magnetic settling times from approximately 60 s to 10 s. As a result, each action-observation cycle was executed on a fixed 10 s timescale, setting the minimum step duration during training episodes.

The training of the RL agent was organized into episodes, each corresponding to an independent tuning attempt starting from a given machine configuration. The maximum episode length was defined as the maximum number of agent-environment interactions allowed per attempt, and represents a key hyperparameter for balancing exploration and training efficiency. Each interaction consisted of proposing a new action, applying it to the machine via PyEPICS, allowing the system to stabilize (using the overshooting strategy for the main coil), and recording the resulting observations and reward. For Injector 2 training, the maximum episode length was set to 40 steps, which was sufficient to allow the agent to explore corrective actions while keeping training cycles short and compatible with operational constraints. Episodes terminated either when the maximum number of steps was reached or when the cumulative reward surpassed a predefined threshold indicating successful tuning.

To investigate how prior knowledge influences convergence, three complementary training strategies were tested (Fig. 7): (a) RL from scratch, where the agent was initialized with random weights; (b) RL from previous turn, in which the policy learned at one turn number was reused as initialization for the next; and (c) RL from surrogate model, where the actor network was pretrained offline at selected turns using a surrogate derived from historical Injector 2 data, before fine-tuning directly on the machine.

Together, these approaches enabled a systematic assessment of learning performance, policy transfer, and the value of physics-informed pretraining.

VIII. EXPERIMENTAL RESULTS

We evaluated the TD3 agent across five turn configurations spanning nominal and degraded operating modes. Performance was assessed via: (i) convergence time (timesteps and wall-clock), (ii) episode length at convergence

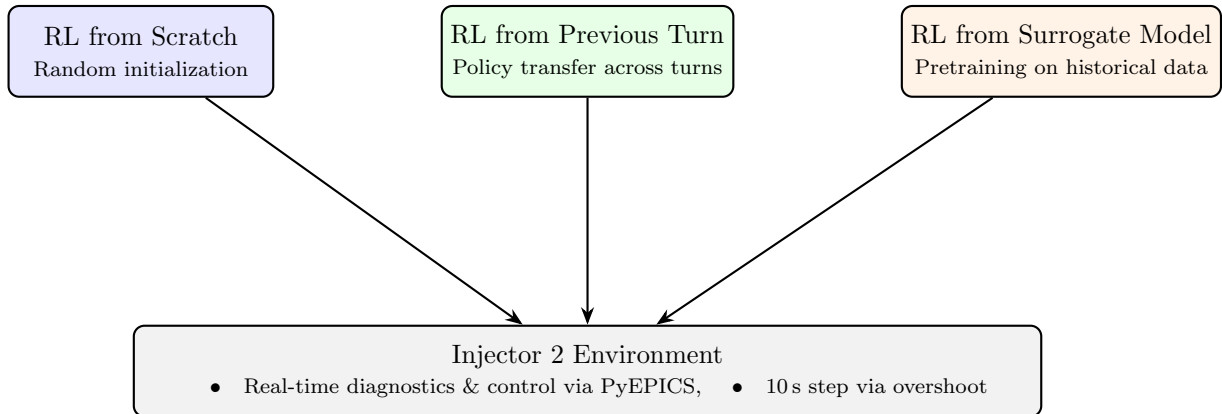


FIG. 7: Overview of the three RL training strategies explored in the Injector 2 experiment: (a) training from scratch with no prior knowledge, (b) initializing from a policy trained at a neighboring turn number, and (c) pretraining with a surrogate model derived from historical data before online fine-tuning.

TABLE III: Summary of TD3 training performance across turns. Convergence time is reported in steps (wall-clock hours).

Turn	Resonators Active	Pretraining	Convergence	Avg. Final Reward	Interlocks	Notable Outcome
72	3 (R1,R2,R3)	No	535 (~ 4.0 h)	-0.06	21 (3 post-conv)	From scratch
73	3 (R1,R2,R3)	Yes	291 (~ 2.3 h)	-0.06	12 (0 post-conv)	Surrogate pretraining
74	3 (R1,R2,R3)	Yes	1117 (~ 5.8 h)	-0.06	51 (3 post-conv)	Transfer from Turn 73
89	2 (R1,R3)	Yes	114 (~ 0.9 h)	-0.055	0	Degraded config; successful
60	4 (R1–R4)	No	217 (~ 2.1 h)	-0.06	4 (1 post-conv)	Nominal config

Convergence is defined as the point after which all episodes solve in ≤ 10 steps.

(target ≤ 10 steps), (iii) final weighted phase error (near-extraction emphasis), (iv) beam losses relative to warning thresholds, and (v) number of interlocks (safety). A consolidated view is provided in Table III.

A. Turn-by-turn RL Training Performance

Turn 72 (baseline, from scratch): This case established the reference performance of the RL agent without any prior information. Starting from random initialization, the agent required about 4 hours (535 steps) to converge. The learning curve in Fig. 8 shows the drop of episode length to ≤ 10 steps with stable final returns. Phase error collapses to within ± 1 degree (Fig. 13, left column, row 1), losses fall well below warning thresholds (right column, row 1), and interlocks are confined to early exploration (Fig. 14, right column, row 1). A total of 21 interlocks were triggered during this training, decreasing to only 3 after convergence.

Beam losses and coil efficiency improved markedly over training. As seen in Fig. 13 (right column, row 1), losses decreased by nearly two orders of magnitude, reaching levels far below the 30 nA warning threshold. In parallel, the mean absolute trim-coil currents were reduced (Fig. 14, left column, row 1), indicating that the agent converged to efficient control strategies that achieve precise phase alignment with minimal corrective action.

Turn 73 (comparison: surrogate pretraining vs. from scratch): At Turn 73, two RL runs were performed under identical machine conditions to directly assess the impact of pretraining. In the first case, the agent was initialized from scratch (random weights), while in the second, the same agent was initialized using a surrogate model pretrained on historical Injector 2 data. This setup enabled a direct, controlled comparison between pretrained and non-pretrained policies for the same turn number.

Relative to Turn 72, the pretrained agent exhibited markedly faster convergence, requiring only about 2.3 hours (291 timesteps), while achieving equivalent final performance (average reward ≈ -0.06). The learning curve in Fig. 9 shows a rapid stabilization of episode length to fewer than ten steps, with the reward reaching its steady value within the first few episodes. Phase alignment accuracy remained within $\pm 1^\circ$ of the reference (Fig. 13, left column, row 2), losses stayed well below the 30 nA warning threshold (right column, row 2), and interlocks disappeared entirely after

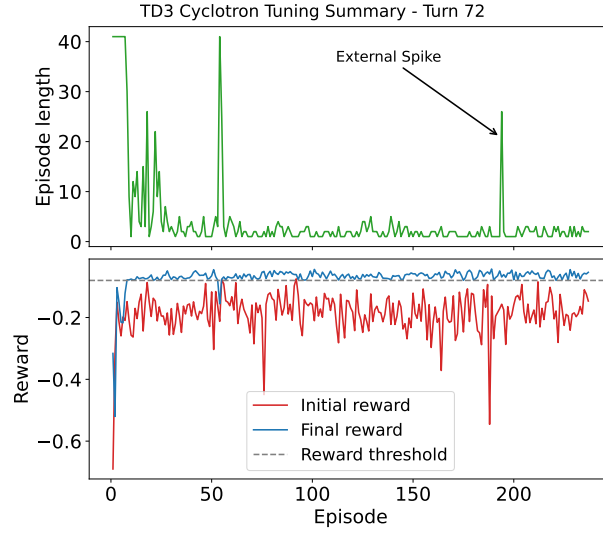


FIG. 8: Learning Curve for Turn 72: Top Plot, Episode Length during TD3 Training; bottom Plot, Reward evolution across episodes. Total training time is 960 timesteps, totaling 7 hours from start-to-end.

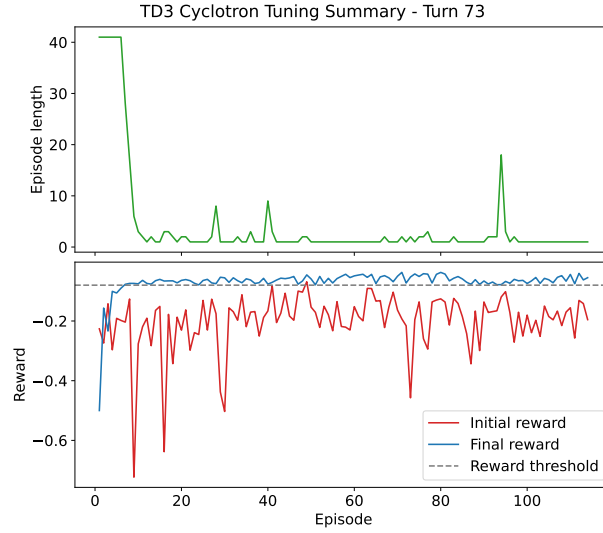


FIG. 9: Learning Curve for Turn 73 with pretraining: Top Plot, Episode Length during TD3 Training; bottom Plot, Reward evolution across episodes. Total training time is 460 timesteps, totaling 3.9 hours from start-to-end.

early exploration (Fig. 14, right column, row 2).

A direct comparison of the two training runs for Turn 73 confirmed the benefit of surrogate pretraining: the surrogate-initialized policy reached stable high rewards within a few episodes, whereas the agent trained from scratch exhibited larger fluctuations and slower convergence. Overall, surrogate-based pretraining provided a safer and more efficient initialization, enabling faster learning, smoother convergence, and stable operation throughout.

Turn 74 (transfer from Turn 73): This experiment tested policy transfer by initializing the TD3 agent with the actor network trained at Turn 73. Despite the warm start, the agent faced markedly different beam dynamics, in particular a smaller turn separation near extraction.

As a result, adaptation required roughly 50 episodes before the policy stabilized, leading to the longest overall convergence time among all investigated turns (5.8 hours, 1117 steps). The learning curve in Fig. 10 shows an initially slow improvement followed by steady convergence, with final rewards around -0.06 . In addition, Turn 74 exhibited the highest number of interlocks among all runs, 51 in total, with three occurring after convergence (Fig. 14, right column, row 3).

Phase alignment accuracy remained within $\pm 1.5^\circ$ of the reference (Fig. 13, left column, row 3), and beam losses, initially above 10 nA, were successfully reduced below 1 nA after convergence (right column, row 3), though overall

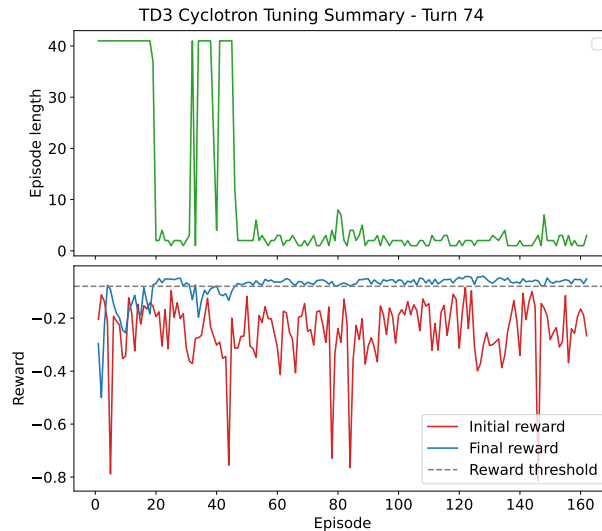


FIG. 10: Learning Curve for Turn 74: Top Plot, Episode Length during TD3 Training; bottom Plot, Reward evolution across episodes. Total training time is 1500 timesteps, totaling 7.8 hours from start-to-end.

loss suppression remained less effective than at Turn 72 and 73. Simultaneously, the mean trim-coil usage steadily decreased (Fig. 14, left column, row 3), indicating efficient control once adaptation was achieved.

Overall, while the agent ultimately achieved stable tuning and satisfactory reward performance, the extended adaptation time and elevated interlock rate highlight the limited generalization of policies across turns and the strong influence of underlying turn-dependent dynamics discussed in Sec. V.

Turn 89 (comparison: surrogate pretraining vs. from scratch): Turn 89 represented the most degraded configuration, with only two resonators active, resulting in smaller turn separation and high beam-loss sensitivity. As in Turn 73, surrogate pretraining was directly compared to training from scratch to evaluate the impact of historical-data initialization. Contrary to expectations, the pretrained agent exhibited unstable learning dynamics, larger reward fluctuations, and slower convergence toward the target threshold. In contrast, the agent trained from scratch achieved faster and more reliable convergence (~ 0.9 hours, 114 steps) without any interlocks (Fig. 11).

Phase alignment accuracy remained within $\pm 1.5^\circ$ of the reference (Fig. 13, left column, row 4), and beam losses were reduced by nearly two orders of magnitude, reaching sub-nA levels after convergence (right column, row 4). Coil activity stabilized accordingly, with no excessive actuation (Fig. 14, left column, row 4).

The poorer performance of the surrogate-pretrained model highlights the limitations of applying pretraining under substantially altered beam dynamics or machine setups. These findings emphasize that successful pretraining requires accurate regime matching between the surrogate domain and the target operational state.

Turn 60 (nominal, all resonators): The nominal configuration with all four resonators active provided the most stable operating regime and served as a benchmark for the RL framework. Without any pretraining, the agent converged in approximately 2.1 hours (217 steps) with only four interlocks, confirming the robustness and efficiency of online learning under nominal conditions. The episode and reward evolution in Fig. 12 demonstrate rapid convergence within fewer than 20 episodes, with smooth and stable final rewards. Phase alignment accuracy remained within $\pm 1.5^\circ$ of the reference (Fig. 13, left column, row 5), while beam losses steadily decreased and remained well below operational thresholds after convergence (right column, row 5). Trim-coil usage was consistently low (Fig. 14, left column, row 5), indicating that the agent benefited from the larger turn separation to maintain high beam quality with minimal corrective intervention. These results establish Turn 60 as a strong baseline for reliable RL-based tuning and confirm that the learning framework performs most effectively under well-separated beam dynamics.

Summary and Outlook. Across all investigated turn configurations, the TD3-based RL framework consistently achieved stable and reproducible tuning of the Injector 2 cyclotron within a few hours of online training (typically under 1000 timesteps). The experiments demonstrated that, once equipped with an appropriate reward formulation and interlock-aware safety layer, the RL agent was capable of reliably aligning beam phases, suppressing losses, and minimizing corrective actions across varying operational regimes. Pretraining using surrogate data proved beneficial under comparable machine conditions (e.g., Turn 73), but introduced bias under strongly altered dynamics (Turn 89), highlighting the importance of accurately matching simulation and real-machine behavior. Furthermore, policy transfer between turns (Turn 73 \rightarrow 74) was found to be limited, confirming that turn-dependent beam dynamics require localized adaptation. Overall, these results establish RL as a viable and safe control paradigm for real-time cyclotron

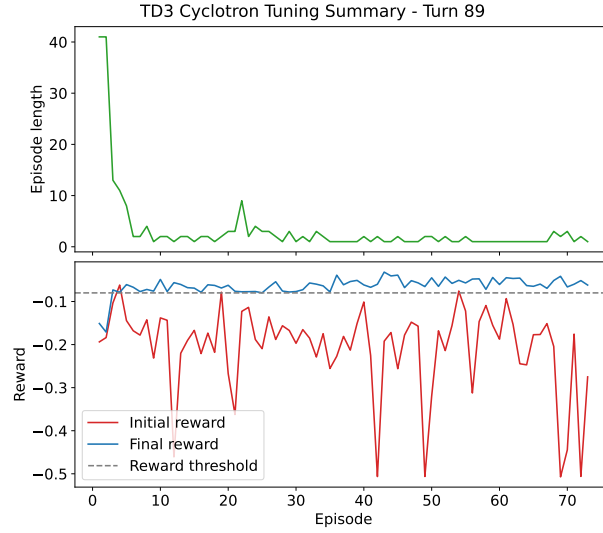


FIG. 11: Learning Curve for Turn 89: Top Plot, Episode Length during TD3 Training; bottom Plot, Reward evolution across episodes.

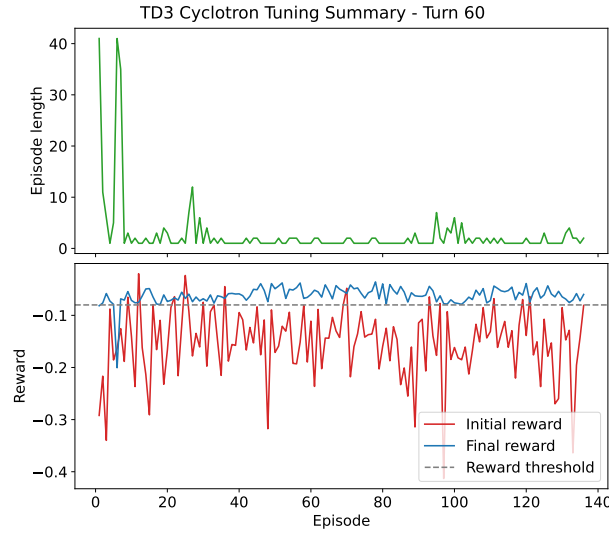


FIG. 12: Learning Curve for Turn 60: Top Plot, Episode Length during TD3 Training; bottom Plot, Reward evolution across episodes.

tuning.

B. Overnight Evaluation and Reliability Testing

To assess the reliability and robustness of the trained RL policy under realistic accelerator operation, the TD3 agent was deployed in evaluation mode on the Injector 2 cyclotron during a series of overnight runs conducted after daytime training sessions. In this mode, the agent acted in a purely deterministic manner, executing its learned policy few hours earlier without further gradient updates or exploration noise, thus directly testing its capacity for autonomous stabilization and long-term control.

The evaluation was performed across three representative configurations: Turn 74 (three resonators active), Turn 89 (two resonators active), and Turn 60 (four resonators active). These settings span increasing levels of operational stability and beam-loading complexity, providing a stringent test of the policy’s generalization capability. During each overnight session, the agent retained full control of the trim coils, main correction coil (AIHS), and resonator voltage (CI3V). To emulate realistic machine drifts, small random perturbations (“kicks”) were occasionally introduced in

the actuator setpoints, allowing assessment of the agent’s ability to autonomously recover optimal beam conditions.

1. Agent Response to Drifts and Perturbations

Figure 15 summarizes the evolution of the initial and final rewards throughout the evaluation for Turns 74, 89, and 60. Across all configurations, the agent consistently maintained stable operation and promptly corrected perturbations, restoring the system to high-reward conditions without triggering any interlocks.

For Turn 74, the first configuration tested, the reward threshold was conservatively kept at its training value of -0.08 , while for Turns 60 and 89, the threshold was tightened to -0.06 to further penalize beam losses and incentivize the agent to improve its tuning. In every case, the final reward remained above the threshold, demonstrating the policy’s ability to maintain beam quality despite external disturbances and drifts. The difference between initial and final rewards illustrates the closed-loop corrective response, confirming that the trained RL policy can stabilize the cyclotron in real time under natural drifts and hardware fluctuations.

2. Interlock Behavior and Recovery Performance

The evolution of beam losses during these tests is shown in Fig. 15. For Turn 74, a gradual increase in beam losses was observed overnight, although no interlocks were triggered and the system remained under stable control. A brief retraining session (approximately 30 minutes) performed the following day successfully restored losses to near-zero levels, demonstrating that short, targeted updates suffice to recover optimal performance.

In contrast, for Turns 60 and 89, where the higher reward threshold of -0.06 was applied, the agent maintained both low beam losses and stable coil usage throughout the evaluation. These results confirm that the trained RL policy not only preserves safe operation over extended periods but also autonomously compensates for small disturbances without human intervention.

3. Discussion

The overnight evaluation results confirm that the RL-based control framework generalizes reliably beyond its training conditions. The policy demonstrated strong resilience to environmental drifts, maintained beam stability across a range of operating regimes, and operated fully autonomously for several hours without triggering interlocks. Furthermore, the ability to restore performance via brief retraining underscores the value of intermittent fine-tuning as a sustainable long-term operation strategy. These findings highlight the readiness of RL-based tuning for deployment in continuous operation modes of high-power proton cyclotrons, where reliability, adaptability, and safety are critical.

C. Generalization to Higher Current

The final phase of the campaign assessed the ability of the RL model, trained exclusively under low-current conditions at $20\text{ }\mu\text{A}$, to generalize when evaluated at higher beam currents. Experiments were conducted with all four resonators active, corresponding to a 60-turn configuration representing nominal operation conditions. The beam current was systematically increased following a Fibonacci-like ramp-up sequence ($100, 200, 300, 500$, and $800\text{ }\mu\text{A}$), within a continuous evaluation interval of approximately 1.5 hours.

At every current level, the system was first perturbed by random variations of actionable parameters within the predefined exploration space. The RL agent was then tasked with restoring optimal beam conditions by maximizing the reward function, which implicitly minimized beam losses. As in previous stages of the campaign, success was defined by surpassing the reward threshold of -0.08 , after which the agent continued monitoring and fine-tuning. Across all high-current tests, the RL agent restored the beam in at most five steps and no interlocks were triggered, confirming its robustness and safety. A summary of results is provided in Table IV.

As the current exceeded $300\text{ }\mu\text{A}$, modest but expected complications were noted. Beam size and position shifts are inherent to the physics of increasing beam current. These effects made the system more sensitive to perturbations and rendered the random reset procedure less straightforward. In some instances, unsafe parameter combinations from the reset logic triggered interlocks before the RL agent could act. Although not a major issue, this required attention: the action space was narrowed and the maximum permissible step size reduced, enabling stable recovery while preserving adaptability.

TABLE IV: Performance of the RL model at increasing beam currents.

Current (μA)	Initial Reward	Final Reward	Initial Losses (nA)	Final Losses (nA)	Adjustment Steps
50	-0.14	-0.041	0.2	0.2	1
100	-0.25	-0.046	2.0	0.2	3
200	-0.12	-0.049	0.2	0.2	1
300	-0.77	-0.060	95.0	0.3	3
500	-0.33	-0.062	7.0	0.2	3
800	-0.54	-0.069	23.3	0.3	5

In summary, the results demonstrate that the RL model generalizes reliably to higher-current conditions up to the maximum tested level of 800 μA . The increased beam sensitivity highlights the importance of adaptive action space tuning and parameter scaling when extending RL-based control to higher-intensity regimes.

IX. CONCLUSION

The present study demonstrates, for the first time, that reinforcement learning (RL) can be reliably deployed for autonomous closed-loop tuning of a high-power cyclotron. Through a series of controlled experiments on Injector 2 at PSI, the TD3 agent successfully optimized beam phase and losses across five turn configurations, encompassing both nominal and degraded operating regimes. These results show that ML-based control can operate within strict safety boundaries while achieving convergence within a few hours, even under varying machine conditions.

From a methodological standpoint, the experiments addressed several fundamental questions regarding algorithm design, observability, and transferability. The TD3 framework proved particularly suitable for this task, striking a balance between sample efficiency and operational safety in a multi-dimensional continuous control space. The use of phase and loss signals as state variables provided an effective, physically meaningful representation of the beam-machine interaction. Action-space analysis confirmed that AIHS (main field) and CI3V (cavity voltage) dominated the beam phase response, while the trim coils served as fine-correction channels, enabling efficient control with minimal intervention.

Pretraining emerged as a valuable, though context-dependent acceleration strategy. When the surrogate data reflected conditions close to the real setup (as at Turn 73), convergence was significantly faster and safer than from random initialization. Conversely, in degraded configurations (Turn 89), pretraining introduced a bias that impeded adaptation, underscoring the need for careful alignment between surrogate models and the real operating regime. This interplay between model fidelity and learning efficiency highlights the importance of combining physics-based surrogate models with adaptive, online retraining for robust deployment.

Across all configurations, convergence trends mirrored those predicted by single-particle simulations, validating the use of physics-informed RL environments for pre-experiment benchmarking. Furthermore, policy robustness was confirmed during overnight evaluation runs, where the trained agents maintained beam stability and corrected imposed perturbations autonomously, without triggering interlocks. This establishes not only the feasibility but also the repeatability of ML-based tuning under real operating conditions.

Importantly, the campaign revealed that policies do not generalize across turn numbers without adaptation. This is fully consistent with the turn-dependent beam dynamics discussed in Sec. V. However, warm-starting from previous policies and targeted retraining substantially reduced adaptation time, pointing toward the viability of hierarchical or multi-turn RL frameworks for future deployment.

A further step toward operational generalization was demonstrated through high-current tests, where the RL policy trained exclusively at 20 μA maintained stable and low-loss operation up to 800 μA (≈ 58 kW average beam power). The agent consistently restored optimal beam conditions in fewer than five steps at all current levels, without triggering interlocks. At higher currents, increased beam sensitivity introduced mild operational challenges, mainly related to random reset perturbations and loss of margin in the action space, but these were successfully mitigated through adaptive step-size control. This scaling experiment confirms that the learned policy generalizes robustly across current-dependent space-charge regimes, provided the action normalization and safety constraints are appropriately tuned. Such robustness is a key prerequisite for extending ML-based control to the megawatt-class HIPA cyclotron and, ultimately, to ADS-grade accelerator systems.

Looking forward, these findings provide a solid foundation for scaling the approach to the full HIPA complex and, ultimately, to accelerator-driven systems (ADS). The path toward HIPA integration will follow a staged, safety-certified roadmap: (i) simulation-first validation of each subsystem, (ii) modular agent design combining operational and safety controllers, and (iii) incremental deployment under operator supervision. The broader goal is to establish a

transparent, certifiable ML control architecture capable of sustaining long-term, high-current operation with minimal human intervention. Such a system would not only enhance operational reliability for HIPA but also address the stringent autonomy and fault-tolerance requirements of ADS-class accelerators.

In summary, this work provides compelling evidence that reinforcement learning can transition from simulation to real-machine control in a safe, interpretable, and operationally meaningful way. By coupling physical modeling with adaptive optimization, the approach paves the way for intelligent, self-correcting accelerator control systems, an essential step toward the next generation of high-power proton drivers.

Acknowledgments

The authors acknowledge the support of the PSI management and the Transmutex management for enabling and supporting this experimental campaign. We thank Christian Baumgarten, Mariusz Sapinski, Luciano Calabretta, Rudolf Dölling, and Jilei Sun for valuable discussions. Special thanks are extended to the PSI control room crew for their essential support during the Injector 2 experimental campaign. The main author also wishes to thank Verena Kain and Michael Schenk for insightful discussions and feedback during the CERN School of Computing, which helped shape several aspects of this work.

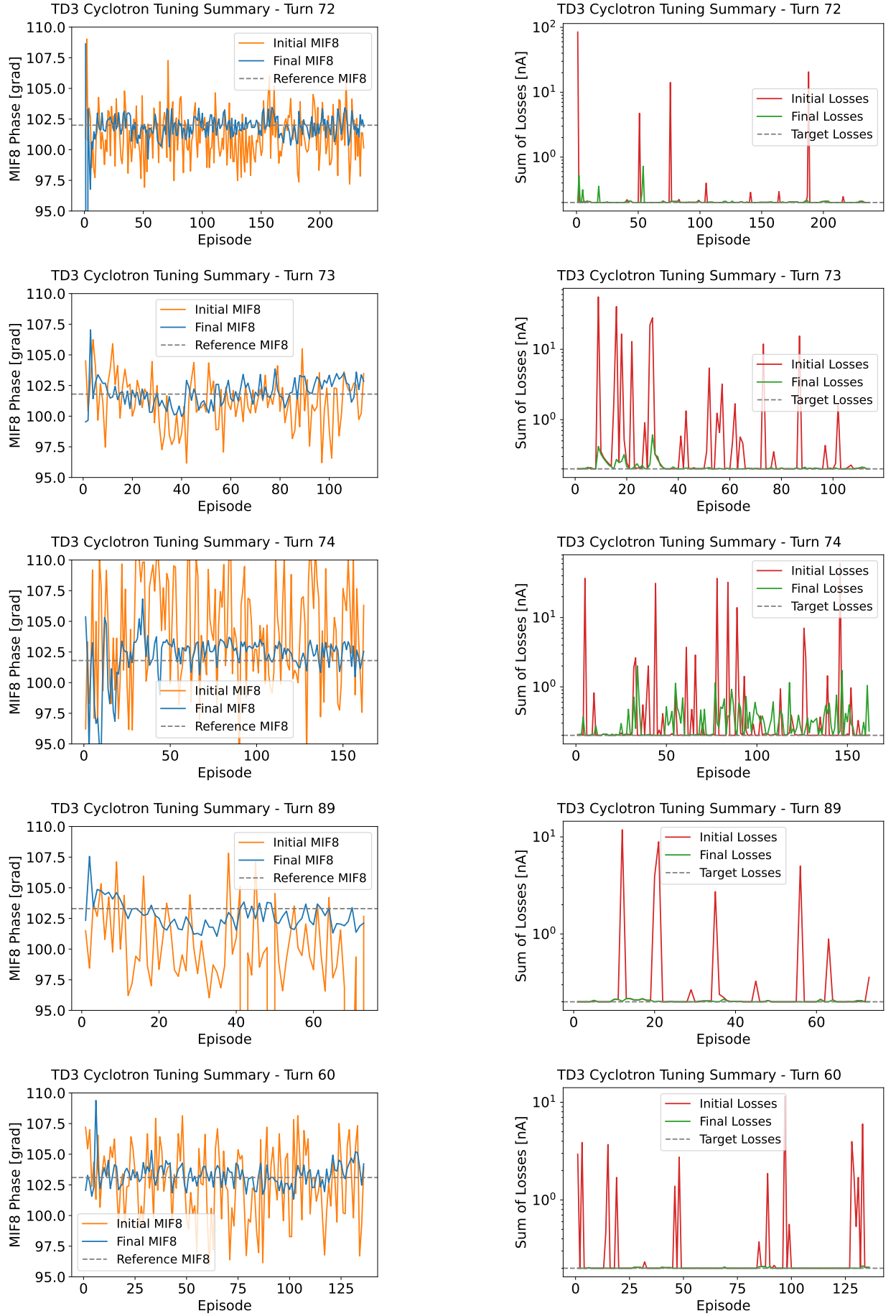


FIG. 13: Summary across five turn configurations (top to bottom: 72, 73, 74, 89, 60). Left column: phase-alignment performance (MIF8 at extraction) versus training episode. Right column: beam losses at extraction versus training episode. Initial denotes the machine state before the agent's first action. Final represents the last state reached by the RL agent at the end of the episode.

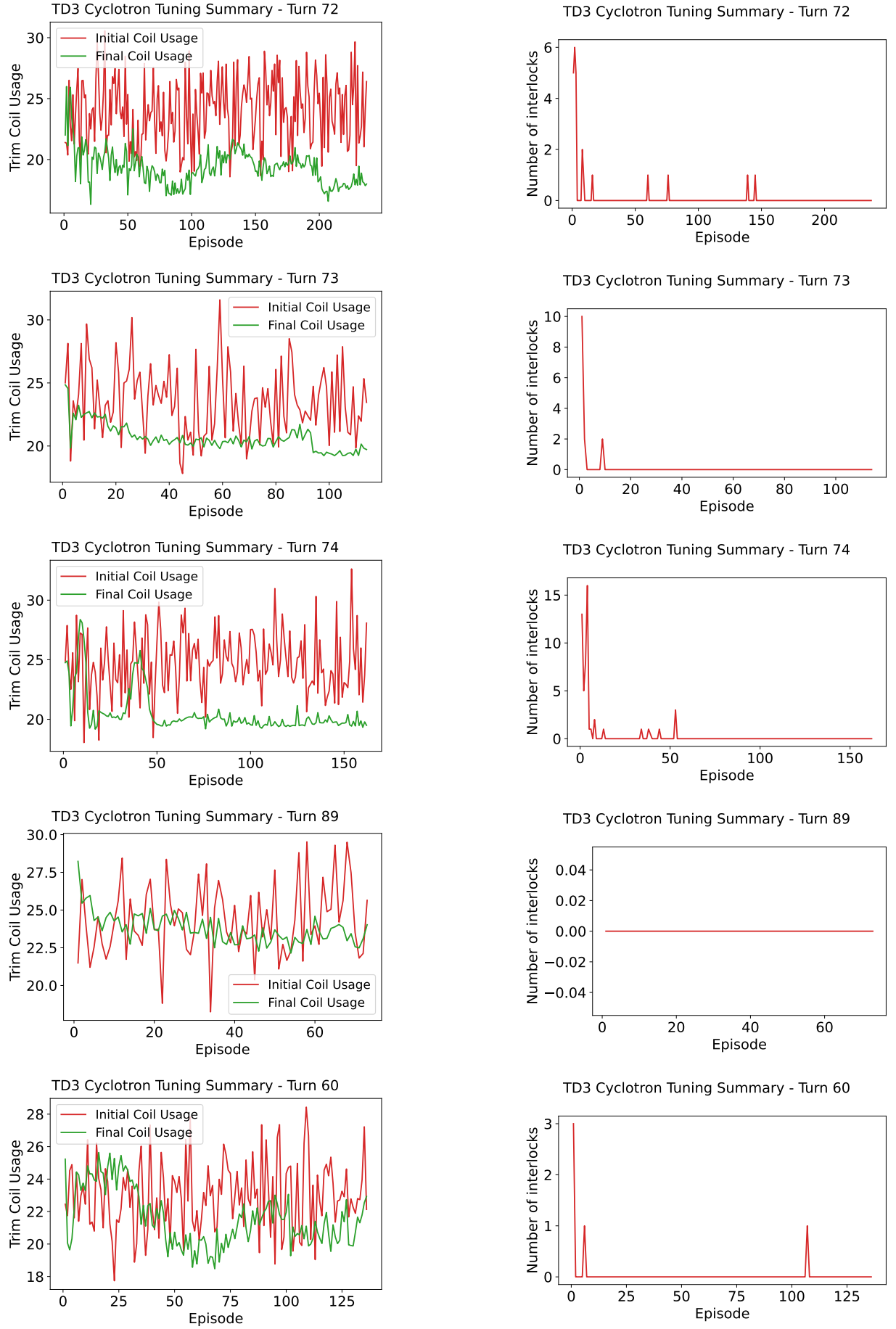


FIG. 14: Summary across five turn configurations (top to bottom: 72, 73, 74, 89, 60). Left column: coil usage versus training episode. Right column: number of interlocks versus training episode. All cases converge to the operational targets; see text for per-turn details.

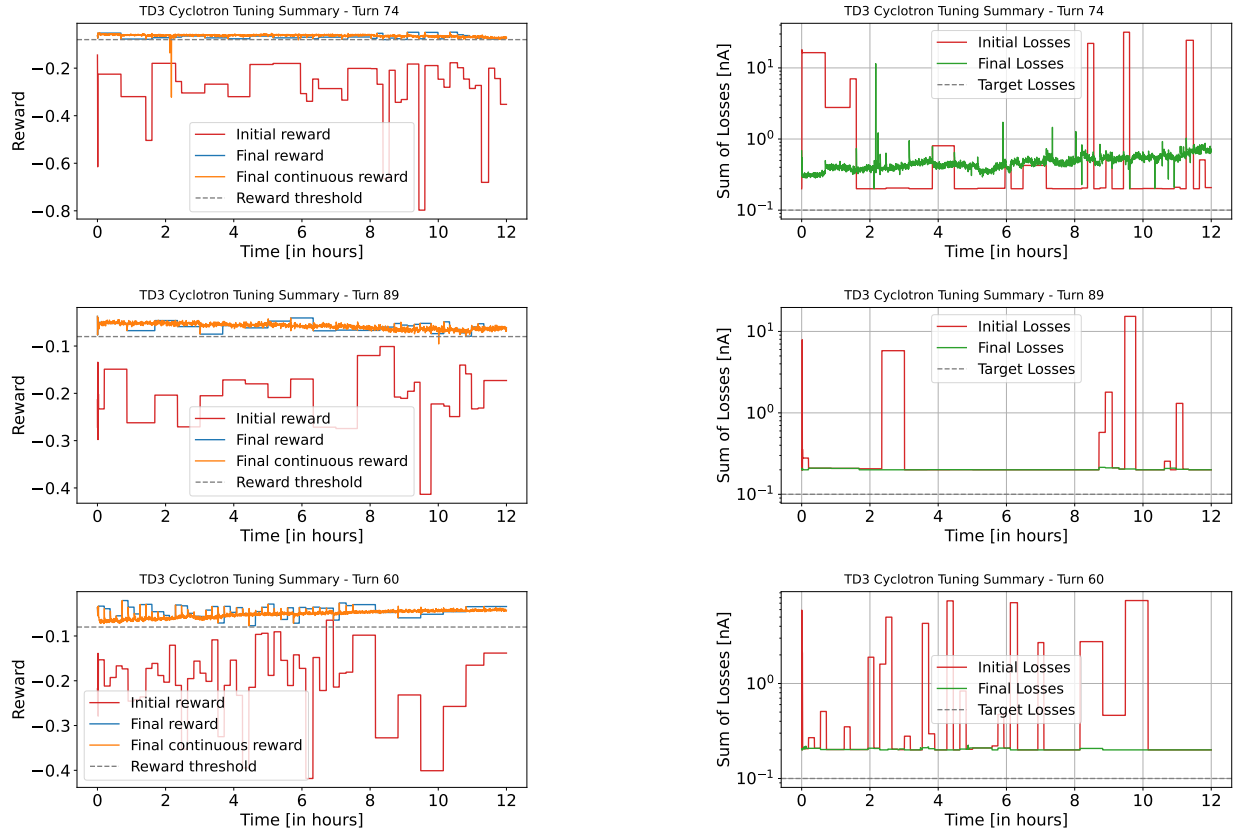


FIG. 15: Overnight evaluation of the trained TD3 policy across three representative configurations (top to bottom: Turns 74, 89, and 60). Left column: evolution of initial and final rewards during continuous, autonomous operation.

Right column: corresponding beam loss evolution over the same intervals. In all cases, the agent successfully maintained high-reward, low-loss operation, autonomously compensating for perturbations without triggering interlocks.

FIG. 16: Main features correlation heatmap (temperature sensors correlations highlighted).

-
- [1] J. Grillenberger, C. Baumgarten, and M. Seidel, SciPost Physics Proceedings p. 002 (2021).
 - [2] D. Kiselev, P.-A. Duperrex, S. Jollet, S. Joray, D. Laube, D. Reggiani, R. Sobbia, and V. Talanov, SciPost Physics Proceedings p. 003 (2021).
 - [3] C. Rubbia, C. Roche, J. A. Rubio, F. Carminati, Y. Kadi, P. Mandrillon, J. P. C. Revol, S. Buono, R. Klapisch, N. Fiétier, et al., Tech. Rep. (1995).
 - [4] H. A. Abderrahim, P. Baeten, D. De Bruyn, and R. Fernandez, Energy conversion and management **63**, 4 (2012).
 - [5] M. Haj Tahar, *Fault-compensation scheme in cyclotrons*, Talk at the 2024 Workshop on Fixed Field Alternating Gradient Accelerators (FFA24) (2024), URL <https://indico.rcnp.osaka-u.ac.jp/event/2375/contributions/13823/>.
 - [6] A. Edelen and X. Huang, Annual Review of Nuclear and Particle Science **74**, 557 (2024), ISSN 1545-4134, URL <https://www.annualreviews.org/content/journals/10.1146/annurev-nucl-121423-100719>.
 - [7] A. L. Edelen, N. Neveu, M. Frey, and et al., in *Proc. IPAC'18* (2018), pp. 2066–2069.
 - [8] A. Scheinker and X. Huang, Phys. Rev. Accel. Beams **23**, 124801 (2020).
 - [9] M. Aiba, M. Schenk, Y. Li, and et al., Phys. Rev. Accel. Beams **22**, 082802 (2019).
 - [10] S. Hirländer, T. Hellert, N. R. Lobanov, and et al., Nucl. Instrum. Methods Phys. Res. A **1048**, 167926 (2023).
 - [11] J. Stetson, S. Adam, M. Humbel, W. Joho, and T. Stammach, in *Proceedings of the 13th International Conference on Cyclotrons and their Applications* (1992), pp. 36–39.
 - [12] M. Schneider, J. Grillenberger, et al., in *Proc. of the 22nd International Conference on Cyclotrons and their Applications, Cape Town, South Africa* (2019), pp. 123–126.
 - [13] C. Baumgarten and H. Zhang, in *68th Advanced Beam Dynamics Workshop on High-Intensity and High-Brightness Hadron Beams (HB'23), Geneva, Switzerland, 09-13 October 2023* (2024), pp. 547–550, URL <https://proceedings.jacow.org/hb2023/papers/thbp34.pdf>.
 - [14] C. Baumgarten, Physical Review Special Topics—Accelerators and Beams **14**, 114201 (2011).
 - [15] D. Sagan, Nucl. Instrum. Methods Phys. Res. A **558**, 356 (2006).
 - [16] A. Parfenova, M. Humbel, A. Petrenko, A. Mezger, and C. Baumgarten, in *Proceedings of the 7th International Particle Accelerator Conference (IPAC'16)* (JACoW, Busan, Korea, 2016), p. TUPMR019, cERN-ACC-2016-277.
 - [17] S. Fujimoto, H. Hoof, and D. Meger, in *Proc. ICML 2018* (2018), pp. 1587–1596, URL <https://proceedings.mlr.press/v80/fujimoto18a.html>.
 - [18] V. Kain, S. Hirlander, B. Goddard, F. M. Velotti, G. Z. Della Porta, N. Bruchon, and G. Valentino, Phys. Rev. Accel. Beams **23**, 124801 (2020), URL <https://link.aps.org/doi/10.1103/PhysRevAccelBeams.23.124801>.
 - [19] R. S. Sutton and A. G. Barto, *Reinforcement Learning: An Introduction* (MIT Press, 2018), 2nd ed.